Published in final edited form as:
Brain Behav Immun. 2013 August ; 32: 9–18. doi:10.1016/j.bbi.2013.03.003.

Sustained IL-1β expression impairs adult hippocampal neurogenesis independent of IL-1 signaling in nestin+ neural precursor cells

Michael D. Wu, **Sara L. Montgomery**, **Fatima Rivera-Escalera**, **John A. Olschowka**, and **M. Kerry O'Banion***
Department of Neurobiology & Anatomy, University of Rochester School of Medicine &Dentistry, Rochester, NY 14642

Abstract

Alterations in adult hippocampal neurogenesis have been observed in numerous neurological diseases that contain a neuroinflammatory component. Interleukin-1β (IL-1β) is a pro-inflammatory cytokine that contributes to neuroinflammation in many CNS disorders. Our previous results reveal a severe reduction in adult hippocampal neurogenesis due to focal and chronic expression of IL-1β in a transgenic mouse model, IL-1β^{XAT}, that evokes a complex neuroinflammatory response. Other investigators have shown that IL-1β can bind directly to neural precursors to cause cell cycle arrest in vitro. In order to observe if IL-1 signaling is necessary in vivo, we conditionally knocked out MyD88, an adapter protein essential for IL-1 signaling, in nestin^{+} neural precursor cells (NPCs) in the presence of IL-1β-dependent inflammation. Our results show that conditional knockout of MyD88 does not prevent IL-1β-induced reduction in neuroblasts using a genetic fate mapping model. Interestingly, MyD88 deficiency in nestin^{+} NPCs causes an increase in the number of astrocytes in the presence of IL-1β, suggesting that MyD88-dependent signaling is important in limiting astroglial differentiation due to inflammation. MyD88 deficiency does not alter the fate of NPCs in the absence of inflammation. Furthermore, the inflammatory milieu due to IL-1β is not affected by the absence of MyD88 in nestin^{+} NPCs. These results show that sustained IL-1β causes a reduction in adult hippocampal neurogenesis that is independent of MyD88-dependent signaling in nestin^{+} NPCs, suggesting an indirect negative effect of IL-1β on neurogenesis.

Keywords

neuroinflammation; interleukin-1; adult; neurogenesis; astrocytes; nestin; MyD88

1. Introduction

In the adult brain, neurogenesis occurs in the subventricular zone of the lateral ventricles and the subgranular zone (SGZ) of the dentate gyrus in the hippocampus. Within the SGZ,

*Corresponding Author: M. Kerry O'Banion, MD, PhD, 601 Elmwood Avenue, Box 603, University of Rochester Medical Center, Rochester, NY 14642, Phone: 585 275-5185, FAX: 585 756-5334, kerry_obanion@urmc.rochester.edu.

Conflict of Interest Statement: All authors declare that there are no conflicts of interest.

nestin^{+} neural precursor cells (NPCs) give rise to transient amplifying daughter cells that in turn produce neuroblasts (Encinas et al., 2006; Seri et al., 2001). Neuroblasts can be identified by their expression of markers associated with neuronal migration, e.g. doublecortin (DCX). Once a neuroblast reaches its destination, it downregulates these migrational markers and expresses markers of mature neurons, e.g. NeuN. Adult hippocampal neurogenesis is involved in changes in behavior such as stress (Ben Menachem-Zidon et al., 2008; Koo and Duman, 2008; Lagace et al., 2010), depressive-like behavior (David et al., 2009; Sahay and Hen, 2007), and learning and memory (Cao et al., 2004; Clark et al., 2008; Deng et al., 2009; Leuner et al., 2004; Shors et al., 2001; van Praag et al., 1999). Furthermore, traumatic brain injury, epilepsy, stroke, and neurodegenerative diseases are all CNS disorders with alterations in adult neurogenesis (Kaneko and Sawamoto, 2009). The pro-inflammatory cytokine interleukin (IL)-1 is implicated in all of these disorders and prior evidence indicates that increased IL-1 negatively impacts adult hippocampal neurogenesis (Allan et al., 2005; Ben Menachem-Zidon et al., 2008; Gemma et al., 2007; Goshen et al., 2008; Koo and Duman, 2008).

The IL-1 family consists of two agonists, IL-1α and IL-1β, and a naturally occurring antagonist, IL-1 receptor antagonist (IL-1Ra). IL-1β is the main secreted agonist that signals via the type 1 IL-1 receptor (IL-1R1). IL-1 binding to IL-1R1 results in recruitment of various signaling mediators beginning with myeloid differentiation primary response protein 88 (MyD88), induction of mitogen activated protein kinase pathways, and activation of transcription factors (Sims and Smith, 2010; Takeda and Akira, 2004; Wesche et al., 1997). IL-1 acts on resident CNS cells to induce expression of other cytokines and chemokines, activate glia such as microglia and astrocytes, and recruit peripheral leukocytes to invade the brain (Allan et al., 2005). The IL-1 family is an ideal system to understand the effect of a pro-inflammatory cytokine on adult hippocampal neurogenesis due to a well characterized signaling cascade and a single receptor with a high density in the hippocampus (Cunningham et al., 1992).

Prior evidence shows that adult hippocampal NPCs in the SGZ express IL-1R1 in vivo and undergo cell cycle arrest when exposed to IL-1β in vitro (Koo and Duman, 2008; McPherson et al., 2011). In addition, we recently demonstrated in vivo that sustained expression of human IL-1β in the adult hippocampus results in a robust reduction of hippocampal neurogenesis by skewing NPCs toward astroglial differentiation in transgenic mice engineered to chronically express human IL-1β following viral transduction of Cre-recombinase (Wu et al., 2012). Moreover, bilateral IL-1β overexpression in this IL-1β^{XAT} mouse model leads to deficits in learning and memory in the Morris water maze and in a contextual fear conditioning task (Hein et al., 2010; Hein et al., 2012; Moore et al., 2009). The mechanism underlying negative regulation of adult hippocampal neurogenesis by IL-1β in vivo is not yet known. Therefore, we set out to test the hypothesis that IL-1β signaling in nestin^{+} neural precursor cells is required for IL-1β's ability to inhibit neurogenesis by inducing a conditional knockout of MyD88, which is necessary for IL-1 intracellular signaling, in nestin^{+} cells. For this purpose, we employed a triple transgenic genetic fate mapping model comprised of nestin-CreER^{T2} mice with inducible Cre recombinase activity under a nestin promoter crossed with a Cre-dependent YFP reporter within the Rosa26 locus, and to transgenic mice harboring floxed MyD88 alleles (Lagace et al., 2007; Madisen et al., 2010). Our findings provide insight into IL-1β's effects in vivo on adult hippocampal neurogenesis by demonstrating that these effects are not dependent on intrinsic IL-1 signaling in neural precursor cells to reduce neurogenesis.

2. Methods

2.1. Animals

All protocols were approved by the Institutional Animal Care and Use Committee at the University of Rochester. 10–11 week old nestin-CFPnuc animals were used in the FACS experiment. Nestin-CFPnuc mice express cyan fluorescent protein (CFP) within the nucleus of nestin^{+} cells due to a nuclear localization signal (Encinas et al., 2006). Nestin-CreER^{T2} (Lagace et al., 2007), Ai3-YFP (stock no. 7903, The Jackson Laboratory), and MyD88$^{fl/fl}$ (stock no. 8888, The Jackson Laboratory) mice were used to establish transgenic lines on a C57BL/6 background. Nestin-CreER^{T2} mice contain a transgene expressing Cre recombinase that is sequestered in the cytoplasm by a mutated estrogen receptor. This mutated estrogen receptor translocates to the nucleus in the presence of tamoxifen but not endogenous estrogen. Upon exposure to tamoxifen, Cre recombinase is able to cause recombination between loxP sites within the nucleus. Ai3-YFP mice contain a YFP reporter downstream of a floxed transcriptional stop in the Rosa locus. These reporter mice were designed to exhibit brilliant fluorescence in the CNS (Madisen et al., 2010). MyD88$^{fl/fl}$ mice contain loxP sites on either side of exon 3. Nestin-CreER^{T2} mice were crossed with Cre-dependent YFP reporter mice to yield nestin-CreER^{T2}, EYFP mice (MyD88$^{+/+}$). When these animals are given tamoxifen, YFP is permanently expressed in nestin^{+} cells and any resulting progeny. A subset of these mice were crossed to MyD88$^{fl/fl}$ mice to yield nestin-CreER^{T2}, EYFP, MyD88$^{fl/fl}$, conditional knockout animals (MyD88$^{fl/fl}$). In mice that are floxed for MyD88, treatment with tamoxifen results in an inducible and conditional knockout of MyD88 in nestin^{+} cells. All animals were aged 5–7 weeks old at the beginning of these studies. A subset of animals received intraperitoneal injections of 50 mg/kg BrdU two hours before sacrifice.

2.2. FACS of CFP^{+} cells and detection of MyD88 and IL-1R1

Nestin-CFPnuc or WT mice (n = 2 animals/group) were deeply anesthetized using a mixture of ketamine and xylazine (50 mg ketamine/10 mg xylazine) before decapitation. After the brain was removed, the hippocampi were microdissected in ice-cold 1X HBSS without Mg^{2+} or Ca^{2+}. Single-cell suspensions were prepared using the Neural Tissue Dissociation Kit (Papain) (Miltenyi Biotec #130-092-628, Auburn, CA) and resuspended in 1X HBSS with Mg^{2+} and Ca^{2+}. Sorting was performed immediately on a FACSAria II (BD Biosciences, San Jose, CA) by identifying events with a strong CFP signal, present in nestin-CFPnuc mice but not in WT mice, using either a band pass 450/50 or band pass 550/40 filter. After sorting, RNA was extracted from the samples using Trizol (Ambion #15596018). Samples were incubated in the presence or absence of reverse transcriptase along with oligo dT's and random hexamers using a Superscript III First-Strand Kit (Invitrogen #18080-051). Following reverse transcription, residual RNA was denatured by RNase treatment. MyD88 and IL-1R1 were amplified using the following primers: MyD88 F 5′ ccc tag gac aaa cgc cgg aa 3′; R 5′ aaa gtc ctt ctt cat cgc ctt 3′; IL-1R1 F 5′ tgg agg gac agt ttg gat a 3′; R 5′ gg cat ttt ctc ata gtc ttg g 3′. The annealing temperature for each reaction was 57°C and 52°C for MyD88 and IL-1R1, respectively.

2.3. Construction of recombinant adeno-associated virus serotype 2

The ssIL-1β construct encodes the signal sequence from the human IL-1 receptor antagonist (hIL-1Ra) fused to human IL-1β (hIL-1β) cDNA, producing a mature, secreted hIL-1β that does not require caspase-1 cleavage (Wingren et al., 1996). A ~600 bp fragment containing ssIL-1β was isolated using gel electrophoresis after digestion from a pBSII-KS+ plasmid using BamHI and XhoI. This DNA was then ligated into a shuttle plasmid, pBS-FBR$_{MCS}$, which contains an upstream CMV promoter. This new plasmid, pBS-FBR$_{MCS}$-ssIL-1β, was digested with NotI to yield a 1583 bp fragment containing the CMV promoter, ssIL-1β

construct, and SV40 polyA tail. This fragment was subsequently ligated into the pFBGR plasmid shuttle vector, which contains flanking inverted terminal repeats necessary for virus production. The final plasmid, pFBGR-ssIL-1β, was used to produce recombinant adeno-associated virus serotype 2 using a baculovirus intermediary and S9 cells as previously described (Urabe et al., 2002). Expression of human IL-1β was detected by ELISA using a Quantikine human IL-1β/IL-1F2 Immunoassay (R&D Systems #DLB50, Minneapolis, MN) on supernatants taken from transfected and transduced HEK 293A cells. rAAV2-Phe-scFv was used as a control viral vector; -Phe expresses a single-chain antibody against phenobarbital (Ryan et al., 2010).

2.4. rAAV2 viral titers

For bilateral injections in MyD88$^{+/+}$ and MyD88$^{fl/fl}$ mice, rAAV2-ssIL-1β and rAAV2-Phe-scFv were diluted 33-fold and 100-fold, respectively, in 1X phosphate buffer + 2 mM $MgCl_2$ to yield approximately 2.5x10^8 infectious particles/mL. This concentration was chosen after conducting a pilot study to evaluate viral effects on neuroinflammation and neurogenesis in 8–10 week old WT mice; these animals received unilateral injections with 10-, 100-, and 1000-fold dilutions of rAAV2-ssIL-1β, representing ~10^9, 10^8, and 10^7 infectious particles/mL (Suppl. Fig 1B,C).

2.5. Tamoxifen injections

5–7 week old MyD88$^{+/+}$ (n = 6 females and 6 males) or MyD88$^{fl/fl}$ (n = 15 females and 9 males) animals were injected intraperitoneally daily with 180 mg/kg tamoxifen dissolved in 10% EtOH/90% sunflower seed oil (Sigma-Aldrich #S5007, St. Louis, MO) for 5 days (Lagace et al., 2007). A subset of these animals received intrahippocampal injections (n = 2 females and 4 males for MyD88$^{+/+}$ and n = 9 females and 3 males for MyD88$^{fl/fl}$). Due to the limited production of these genotypes, a proper analysis of sex differences could not be assessed; we did, however, see the same trend in both sexes for all endpoints when we looked at them independently. Given the small sample size, subsequent analyses collapsed data across genders.

2.6. Bilateral rAAV2 injections in MyD88$^{+/+}$ and MyD88$^{fl/fl}$ mice

9–11 week old animals received intrahippocampal viral injections while under isoflurane anesthesia (1.75% isoflurane in 30/70% oxygen/nitrogen gas) using a Kopf stereotactic apparatus. Mice were secured using ear bars and a head holder. Ophthalmic ointment was applied to prevent drying of the eyes. The scalp was disinfected with Betadine prior to incision with a scalpel. Two 0.5 mm burr holds were drilled, one on each side, 1.8 mm caudal and 1.2 mm lateral from Bregma. A 33 gauge needle affixed to a 10 μL syringe (Hamilton, Reno, NV) was lowered over 2 minutes through one hole to a depth of 1.8 mm deep from the dura surface. 2 μL rAAV2 was injected at a rate of 200 nL/min using a Micro-1 microsyringe pump controller (World Precision Instruments, Sarasota, FL). The needle was left in place for 5 minutes to allow for adequate diffusion before being retracted over 2 minutes. The burr hole was filled with bone wax (Ethicon, Somerville, NJ) and the same protocol was followed for the other side. Each animal was injected with rAAV2-ssIL-1beta into the right hippocampus and rAAV2-Phe-scFv into the left hippocampus. Following both injections, the incision was closed with 5-0 suture Dermalon (Covidien, Mansfield, MA). Betadine and topical lidocaine were applied to the top of the suture to prevent infection and for analgesia, respectively. Mice recovered in a heated area before being placed in their home cage. Animals were sacrificed 1 month post viral injection.

2.7. Immunohistochemistry

Animals were deeply anesthetized using ketamine and xylazine (50 mg ketamine/10 mg xylazine) before transcardial perfusion. A perfusate containing 0.15 M phosphate buffer with 0.5% w/v sodium nitrite and 2 IU/mL heparin was flushed through each animal to dilate blood vessels and prevent clotting. This was followed by perfusion with approximately 50 mL of freshly made, ice-cold 4% paraformaldehyde (PFA) in 0.15 M phosphate buffer, pH 7.2. Brains were immersion fixed for 2 h at 4°C, dehydrated overnight in 30% sucrose in 0.15 M phosphate buffer, and snap frozen using dry ice and isopentane. Brains were sectioned in the coronal plane at 30 μm on a sliding microtome into a 24 well plate containing cryoprotectant. Staining of free-floating sections was performed and visualized using Alexa Fluor conjugated secondary antibodies (Invitrogen) and coverslipped with Prolong Gold (Invitrogen #P36930). Primary antibodies are listed in Table 1. Hoechst 33258 (Invitrogen #H3569) staining was used to visualize nuclei for fluorescent images. DCX antigen retrieval was done by microwaving for a total of 15 min in 0.1 M Na Citrate pH 9. Images were captured on a Zeiss Axioplan IIi microscope or Olympus FV1000 laser scanning confocal microscope.

2.8. RNA isolation from hippocampi

One month after viral injection, animals were sacrificed by transcardial perfusion as described above with the omission of the 4% PFA perfusate. After removal of the brain, the hippocampi from these animals were microdissected and snap frozen on dry ice using isopentane. The tissue was homogenized using an Omni Tissue Homogenizer (Omni #LR60902) before Trizol extraction of RNA. Purity was assessed using a spectrophotometer. RNA was reverse transcribed using 2 μg of total RNA in the presence of oligo dT's and random hexamers using a Superscript III First-Strand Kit (Invitrogen #18080-051). After reverse transcription, residual RNA was denatured by RNase H.

2.9. Quantitative Real-Time PCR

Real-time PCR quantification was performed on a Bio-Rad iCycler machine using iCycler iQ software, v3.1. Optimal concentrations for primers as well as probes were empirically determined for each reaction. In general, 20 μL reactions containing 1X iQ Supermix (Bio-Rad #170-8862), 5 nM FITC for background adjustment, custom designed primers (Invitrogen), and FAM-labeled Black Hole Quencher probes (Biosearch Technologies, Novato, CA) were used. Samples were denatured for 3 minutes at 95°C followed by 50 cycles of 30 sec at 95°C and 30 sec at 60°C for denaturation and annealing/elongation, respectively. For TNF-α, the annealing/elongation temperature was 55°C. Threshold counts (Tc) were automatically computed within the exponential phase of each reaction. The efficiency of each reaction was determined using a dilution series of standards for each marker. The amount of 18S RNA was used as a way of standardizing samples. To determine the fold increase of gene X relative to 18S, the following equation was used (adapted from Pfaffl, 2001):

$$=(1+\text{efficiency}^{18S})^{\text{Tc for } 18S}/(1+\text{efficiency}^{X})^{\text{Tc for } X}$$

Sequences for the forward, reverse, and probe oligomers are listed in Table 2.

2.10. Analysis

Injected MyD88$^{+/+}$ and MyD88$^{fl/fl}$ mice were compared to each other as well as non-injected MyD88$^{+/+}$ and MyD88$^{fl/fl}$ animals. For colocalization analyses, the dentate gyrus was outlined as the region of interest at 10X on an Olympus FV1000 laser scanning confocal

microscope. After setting the top and bottom coordinates, multiple z-stacks were imaged using 1 μm thick sections at 60X within this region at a resolution of 512 x 512 pixels. The resulting images were tiled to form a photomontage of the entire area with high resolution. Colocalization of YFP with DCX, NeuN, GFAP, or BrdU was determined using Olympus Fluoview Ver. 2.0c at 60X to ensure proper double labeling within each plane. Analyses were limited to a single coronal section near the inflammatory focus. Statistical significance ($p < 0.05$) was determined by a paired, one-tailed Student's t-test or 2-way analysis of variance (ANOVA) with matching followed by a post-hoc test with a one-tailed Bonferroni adjustment.

Statistical analysis as well as graphs were made using Prism 5 (GraphPad, San Diego, CA). Resizing of images was done using GNU Image Manipulation Program Ver 2.4.7 (gimp.org). Layout was done using vector graphics editor Inkscape Ver 0.48.2 (inkscape.org).

3. Results

3.1. Nestin$^+$ cells isolated from the adult hippocampus express MyD88 and IL-1R1 transcripts

We hypothesized that IL-1β could bind directly to nestin$^+$ cells. Therefore, we wanted to determine whether nestin$^+$ cells expressed the type I IL-1 receptor and its adapter protein, MyD88. We successfully isolated CFP$^+$ cells from hippocampi microdissected from nestin-CFPnuc mice using fluorescence-activated cell sorting. These CFP$^+$ cells were present only in the transgenic animals and not in WT mice (Fig 1A,B). Using cDNA obtained by reverse transcription of RNA purified from these CFP$^+$ cells, we detected expression of the type I IL-1 receptor as well as MyD88 using PCR (Fig 1C,D for MyD88 and IL-1R1, respectively). In contrast, neither of these markers was detected in samples that lacked reverse transcriptase during the cDNA synthesis step. These results indicate that nestin$^+$ neural precursors express critical IL-1β signaling components in the adult brain.

3.2. Intraperitoneal tamoxifen injections successfully label YFP$^+$ cells and their progeny in nestin-CreER^{T2}, YFP mice

Because incorporation of BrdU is not specific to adult neurogenic cells and BrdU becomes undetectable after multiple rounds of division, we decided to use an inducible transgenic model of fate mapping to permanently label nestin$^+$ cells with YFP. We utilized a well characterized model of inducible Cre recombinase under a nestin promoter (Lagace et al., 2007) combined with a Cre-dependent YFP reporter designed for improved fluorescence in the CNS (Madisen et al., 2010). Because the genomic recombination occurred in nestin$^+$ neural stem cells, subsequent progeny from these cells also expressed YFP two months after cessation of tamoxifen (Fig 2A–D). Recombination due to tamoxifen did not occur in all nestin$^+$ cells because DCX$^+$ cells existed that did not express YFP (Fig 2A). Analysis was therefore limited only to cells that were positive for YFP. Neural precursors were identified by incorporation of BrdU given two hours before sacrifice indicating their proliferative nature as well as their location within the SGZ (Fig 2C). Similarly, these cells could be identified by expression of GFAP in their processes (Fig 2D). In contrast to these cells, NeuN$^+$YFP$^+$ cells had multiple branching processes and were located further within the GCL. Animals that lacked either the nestin-CreER^{T2} or YFP transgenes did not express YFP despite tamoxifen injections (data not shown). Therefore, this model provides a method to label cells necessary for adult neurogenesis and their progeny in vivo under inducible and conditional control by tamoxifen.

3.3. Generation of recombinant adeno-associated virus expressing ssIL-1β

We previously demonstrated that IL-1β decreased adult hippocampal neurogenesis and promoted astroglial differentiation in our IL-1β^{XAT} inflammatory model (Wu et al., 2012). Expression of IL-1β by the IL-1β^{XAT} model is dependent on a GFAP promoter (Shaftel et al., 2007b). Because nestin^{+} neural precursors express GFAP, we decided against using this model in our current study. Moreover, the IL-1β^{XAT} model requires transduction of viral-encoded Cre recombinase, an approach that is not compatible with the nestin-Cre-dependent labeling of neural precursor cells in the mice used here. Therefore, we elected to construct an adeno-associated viral vector serotype 2 (AAV2) expressing a ssIL-1β cassette under a CMV promoter. The ssIL-1β construct contains mature human IL-1β coupled with a signal sequence derived from human IL-1 receptor antagonist directing secretion from the transduced cell. This results in constitutive expression of IL-1β that is not enzymatically regulated. Human IL-1β was chosen because it could be differentiated from murine IL-1β. In order to selectively target neurons, AAV serotype 2 was chosen due to its well characterized use in the CNS (Burger et al., 2004; Davidson et al., 2000; Janelsins et al., 2008). ssIL-1β was first cloned into a packaging vector (pFBGR) and transfected into HEK 293A cells to confirm expression of human IL-1β protein. 415.4±36.5 ng/mL hIL-1β was found in the pFBGR-ssIL-1β transfected cells versus 0.6±1.4 ng/mL found in the pFBGR-eGFP control vector ($p=0.0077$, Student's t-test, Supplemental Fig 1A). After packaging, expression of human IL-1β protein was also confirmed following transduction of HEK 293A cells with the rAAV2-ssIL-1β (data not shown, [hIL-1β] > 250 ng/mL). To test its use in vivo, dilutions of rAAV2-ssIL-1β representing approximately 10^7, 10^8 or 10^9 viral particles were unilaterally injected into hippocampi of C57BL/6 mice and stained one month later for DCX, MHC-II, GFAP and neutrophils to qualitatively assess levels neurogenesis and neuroinflammation (Supplemental Fig 1B,C). Based on these results we selected a dose of approximately 2.5 x 10^8 viral particles for all other experiments.

3.4. Conditional knockout of MyD88 does not alter basal neurogenesis in the adult hippocampus

We wanted to determine whether knockout of MyD88 in nestin^{+} cells would affect neurogenesis in the normal adult brain. We labeled nestin^{+} cells with YFP in 5–7 week old MyD88$^{+/+}$ or MyD88$^{fl/fl}$ mice using tamoxifen and sacrificed them two months later (Fig 3A). When we examined YFP^{+} cells two months later for the expression of MyD88 by confocal microscopy, we found no evidence of MyD88 expression in YFP^{+} cells in MyD88$^{fl/fl}$ mice, confirming the conditional knockout (Suppl. Fig 2B). In contrast, MyD88$^{+/+}$ mice showed MyD88 expression in many but not all YFP^{+} cells (Suppl. Fig 2A); MyD88 expression may depend on the age or developmental stage of the cell.

Two months after tamoxifen treatment, the vast majority of YFP^{+} cells developed into NeuN^{+} neurons (Fig 3D). Besides expression of NeuN, these cells were identifiable based on their long processes as well as position within the granule cell layer (Fig 3D). No difference was seen between MyD88$^{+/+}$ or MyD88$^{fl/fl}$ mice regarding the proportion of NeuN^{+}YFP^{+} cells (80.7±5.3% for MyD88$^{+/+}$ and 80.7±2.5% for MyD88$^{fl/fl}$). A smaller subset of YFP^{+} cells were neuroblasts as shown by expression of DCX. DCX^{+}YFP^{+} neuroblasts were mostly present within the SGZ and were rarely found deep within the granule cell layer (Fig 3C). Similar to the NeuN results, there was no difference in YFP^{+} neuroblasts between MyD88$^{+/+}$ and MyD88$^{fl/fl}$ (9.5±2.7% for MyD88$^{+/+}$ and 9.5±1.5% for MyD88$^{fl/fl}$, Fig 3C). Two hours prior to sacrifice, these animals were injected intraperitoneally with BrdU to label proliferating neural precursor cells (Fig 3A). Of the YFP^{+} cells, 1.4±0.4% and 1.1±0.2% were BrdU^{+} in MyD88$^{+/+}$ and MyD88$^{fl/fl}$ animals, respectively, with no significant difference found between genotypes (Fig 3E). BrdU^{+}YFP^{+} cells were almost exclusively confined to the SGZ (Fig 3E). To confirm this finding, we also

stained these animals for GFAP in order to label neural precursors (Fig 3F). Similar to the BrdU results, we found no significant difference in $GFAP^+YFP^+$ cells between $MyD88^{+/+}$ and $MyD88^{fl/fl}$ animals (2.4±0.4% and 3.6±0.8% for $MyD88^{+/+}$ and $MyD88^{fl/fl}$, respectively; $p = 0.31$, Fig 3F). When the total number of YFP^+ cells was compared between $MyD88^{+/+}$ and $MyD88^{fl/fl}$ animals, no significant difference was seen (225±20 and 210±23 cells for $MyD88^{+/+}$ and $MyD88^{fl/fl}$, respectively) suggesting that deletion of MyD88 did not accelerate or decrease the number of cells produced after 2 months (Fig 3B). These results indicated that conditional deletion of MyD88 from $nestin^+$ cells and their progeny did not affect basal neurogenesis in terms of the proportion of proliferating neural precursors, neuroblasts, and mature neurons.

3.5. Knockout of MyD88 in $nestin^+$ cells does not prevent the negative effects of ssIL-1β on neural precursor cells but does result in increased numbers of astrocytes

Based on our previous results and those published by others (Koo and Duman, 2008), we hypothesized that deletion of MyD88 in $nestin^+$ cells would protect neural precursors from the negative effects of IL-1β. To test this hypothesis, we induced YFP expression in $nestin^+$ cells in $MyD88^{+/+}$ and $MyD88^{fl/fl}$ mice using tamoxifen, and after one month injected these animals with rAAV2-Phe-scFv and -ssIL-1β (Fig 4A). When we examined the fate of YFP^+ cells labeled one month previously, we discovered a significant decrease in DCX^+YFP^+ cells by rAAV2-ssIL-1β relative to rAAV2-Phe-scFv for both $MyD88^{+/+}$ and $MyD88^{fl/fl}$ mice (1.4±1.0% and 4.0±1.0%, respectively, for $MyD88^{+/+}$, $p = 0.04$; 1.2±0.5% and 4.9±1.1%, respectively, for $MyD88^{fl/fl}$, $p < 0.01$, Fig 5A). When we quantified the proportion of YFP cells that developed into $NeuN^+$ mature neurons, we found that the majority of YFP cells developed into neurons (Fig 4E). There was a significant decrease in the percentage of $NeuN^+$ cells observed with rAAV2-ssIL-1β in $MyD88^{fl/fl}$ mice (74.6±3.4% and 86.4±2.7%, $p < 0.01$, Fig 5B). We did not, however, detect a difference for $NeuN^+YFP^+$ neurons in $MyD88^{+/+}$ animals (78.4±5.3% and 81.2±5.1%, $p > 0.05$, Fig 5B). Hippocampi that received rAAV2-ssIL-1β had an increase in $GFAP^+YFP^+$ cells when compared to the rAAV2-Phe-scFv side in both genotypes (13.8±4.2% and 6.2±3.2% for $MyD88^{+/+}$, $p = 0.03$; 22.2±3.6% and 3.8±1.1% for $MyD88^{fl/fl}$, $p < 0.001$, Fig 5C). $GFAP^+YFP^+$ cells in hippocampi injected with rAAV2-ssIL-1β had thicker processes as compared to the Phe side, identifying them as reactive astrocytes (Fig 4F). Interestingly, there was a significant interaction between genotype and injection for $GFAP^+YFP^+$ cells ($F(1,15) = 5.362$, $p = 0.04$, Fig 5C). We found a significant increase in the proportion of $GFAP^+YFP^+$ cells between $MyD88^{+/+}$-ssIL-1β and $MyD88^{fl/fl}$-ssIL-1β (13.8 ± 4.2% and 22.2 ± 3.6%, respectively, $p = 0.04$). In contrast, no difference was seen in this population for rAAV2-Phe-scFv between genotypes (6.2 ± 3.2% and 3.8 ± 1.1% for $MyD88^{+/+}$ and $MyD88^{fl/fl}$, respectively, $p = 0.30$). These results indicated that knockout of MyD88 in $nestin^+$ cells and their progeny did not increase the neuroblast or neuron population but did result in more astrocytes, suggesting that MyD88 expression in $nestin^+$ cells limits the development of astrocytes.

3.6. No difference in inflammatory response due to rAAV2-ssIL-1β between $MyD88^{+/+}$ and $MyD88^{fl/fl}$ animals

We wanted to determine whether disrupting IL-1 signaling in $nestin^+$ cells altered the inflammatory response due to rAAV2-ssIL-1β. Therefore, we isolated RNA from hippocampi from $MyD88^{+/+}$ or $MyD88^{fl/fl}$ mice that were injected with rAAV2-ssIL-1β and rAAV2-Phe-scFv. First, we looked at human IL-1β transcript levels in these animals to ensure that viral expression was similar between genotypes. We found no significant difference in human IL-1β transcript levels suggesting similar levels of expression (Fig 6A). When we looked at murine levels of inflammatory cytokines and chemokines/chemokine receptors, we found no significant interaction between genotype and injection. There was,

however, a significant effect of injection suggesting that the type of rAAV2 injection altered inflammatory transcript levels regardless of the presence/absence of MyD88. Post-hoc tests with a Bonferroni adjustment determined that there was no significant difference between $MyD88^{+/+}$ and $MyD88^{fl/fl}$ animals injected with rAAV2-ssIL-1β for mIL-1β, TNF-α, CCL2, CXCL1, and CXCR2 (Fig 6B–F). In conclusion, knockout of MyD88 from $nestin^+$ cells did not alter the inflammatory response due to rAAV2-ssIL-1β.

4. Discussion

The current study supports our previous findings that sustained expression of IL-1β in the hippocampus reduces DCX^+ neuroblasts in the adult brain. This reduction was present in both genotypes suggesting that loss of MyD88 in $nestin^+$ NPCs had no effect on this population. Surprisingly, we did not see a detriment in mature neurons in our $MyD88^{+/+}$ group despite this loss of DCX^+ neuroblasts. This contrasts with our previously published findings in the $IL\text{-}1\beta^{XAT}$ model where fewer BrdU-labeled cells matured into $NeuN^+$ neurons in the presence of IL-1β. Our current study may not have been able to identify a subtle decrease in newly born neurons due to the timing of our experiment. Because we induced recombination in the mice one month before viral injections, a large proportion of YFP^+ cells would have already differentiated into $NeuN^+$ neurons. Therefore, it is likely that we are diluting any effect we see due to the large number of $NeuN^+YFP^+$ cells that developed even before the onset of inflammation with IL-1β. Perhaps if we had chosen a later time point or shortened the interval between tamoxifen treatment and AAV2 IL-1 transduction, the diminished DCX^+ neuroblast population would eventually have led to a decrease in the $NeuN^+$ population.

We had hoped that our genetic model of fate mapping would reveal what happens to $nestin^+$ NPCs in chronic inflammation. Unfortunately, the morphology that defines YFP^+ NPCs is lost due to inflammation. We were unable to detect any $GFAP^+YFP^+$ cells that looked similar to the NPCs seen in the non-injected animals. Furthermore, staining for NPC markers such as nestin was no longer capable of distinguishing these cells; nestin is upregulated by reactive astrocytes and is not specific to NPCs during inflammation (Frisen et al., 1995; Lin et al., 1995). Because of these non-specific markers, it is uncertain whether the $GFAP^+YFP^+$ cells that we have identified are hypertrophic NPCs or reactive astrocytes; given their morphology as well as the robust GFAP staining, it is likely that they are the latter, but we cannot be definitive regarding this without further analysis.

Our results demonstrated that conditional knockout of MyD88 did not alter neurogenesis or the production of astrocytes in animals in the absence of inflammation. In contrast, Rolls et al. found that global deficiency of MyD88 increased the survival of BrdU-labeled cells as well as increased neuronal differentiation within the SGZ (Rolls et al., 2007). In addition, they determined that MyD88 deficiency caused a decrease in the development of $S100\beta^+$ cells but not $GFAP^+$ cells. Furthermore, culturing NPCs in the presence of an inhibitory peptide to MyD88 caused a decrease in the production of βIII^+ new neurons suggesting that MyD88 deficiency is effecting these changes through NPCs and not other cell types. Therefore, their results signify that MyD88 is important in limiting neurogenesis and promoting astrocyte development. A major difference between our study and theirs is that they examined the fate of these cells 7 days after labeling in vivo whereas we looked 2 months later. It is possible that the effect that they observed is transient and diminishes over time. Alternatively, MyD88 activity in other cell types besides $nestin^+$ NPCs and their progeny may be important in regulating neurogenesis and the production of astrocytes.

MyD88 regulation of NPC differentiation may be amplified in the presence of sustained inflammation, which may explain why we see an increase in the production of astrocytes by

NPCs that lack MyD88. This data suggests that MyD88 is involved in inhibiting the differentiation of NPCs into astrocytes in the presence of inflammation. Because MyD88 is involved in numerous signaling cascades, it is unlikely that blocking IL-1R1 signaling is solely responsible for this effect. Since MyD88 is important for TLR signaling, one possibility is inhibition of basal TLR activity in NPCs. TLR2 and TLR4 both signal via MyD88-dependent pathways (Takeda and Akira, 2004). Deletion of TLR2 or TLR4 resulted in opposite effects on adult hippocampal neurogenesis in one study (Rolls et al., 2007). TLR4 deficiency increased neurogenesis and reduced production of astrocytes while TLR2 deficiency antagonized neurogenesis and promoted astrocyte development. Therefore, conditional KO of MyD88 in our model may have promoted astrocyte proliferation through inhibition of TLR2 signaling due to inflammation. Increased proliferation of astrocytes might explain the decrease in $NeuN^+YFP^+$ neurons that is seen only in animals with the conditional knockout of MyD88. This may be explained by the fact that TLR2 signaling is largely dependent on MyD88 while TLR4 signaling can signal through MyD88-independent pathways (Takeda and Akira, 2004). Future studies will have to address whether expression of TLRs is altered in this inducible and conditional model of MyD88 knockout in the context of inflammation.

Here we have shown that murine hippocampal $nestin^+$ NPCs express IL-1R1 and MyD88 suggesting that IL-1β can directly interact with NPCs. This idea was originally put forth by Koo and Duman who showed that acute IL-1β treatment inhibited proliferation of $nestin^+$ NPCs isolated from hippocampi of adult Sprague Dawley rats (Koo and Duman, 2008). Therefore, it is surprising that conditional knockout of MyD88, which is necessary for IL-1R1 signaling, in $nestin^+$ NPCs and their progeny did not alleviate the negative effects of IL-1β in this current study. Our conflicting results may be due to species differences, in vivo versus in vitro disparities, or duration of exposure to IL-1β.

Our current study suggests that another mechanism besides IL-1 is responsible for the changes we see, since disruption of IL-1 signaling via MyD88 knockout had no effect. Other possibilities include pro-inflammatory cytokines such as IL-6 and TNF-α that have been implicated as negative regulators of adult neurogenesis (Iosif et al., 2006; Monje et al., 2003; Vallieres et al., 2002). We have shown that there was an overall significant effect of rAAV2 injection on TNF-α transcript levels suggesting that rAAV2-ssIL-1β increased TNF-α. Furthermore, ssIL-1β expression in another model, the $IL\text{-}1\beta^{XAT}$, increased IL-6 and TNF-α transcript levels (Shaftel et al., 2007b). Inflammatory cells may also be important in mediating the decrease in DCX^+ neuroblasts due to sustained IL-1β. We have previously shown that sustained ssIL-1β expression caused significant glial activation as well as peripheral cell recruitment (Shaftel et al., 2007a; Shaftel et al., 2007b); activation of these various cell types by pro-inflammatory cytokines may negatively affect hippocampal neurogenesis. Furthermore, chemokines are upregulated by ssIL-1β-induced inflammation that would recruit various cell types. Future studies using chemokine ligand/receptor knockouts will aid in deciphering whether a cellular component is responsible. Our findings provide valuable insight into the mechanism of IL-1β's actions on adult hippocampal neurogenesis by highlighting the complex neuroinflammatory environment that involves many other factors beyond IL-1 in regulating neurogenesis.

Supplementary Material

Refer to Web version on PubMed Central for supplementary material.

Acknowledgments

We thank Dr. William Bowers for assistance with generation of the rAAV2 viruses, Dr. Linda Callahan for helping with the confocal imaging, and Drs. Amelia Eisch and Grigori Enikolopov for providing the nestin-CreER^{T2} and nestin-CFPnuc mice, respectively. We also thank Dr. Tanzi Love for advice regarding statistical analyses. Lee Trojanczyk, Jack Walter, and Mallory Olschowka assisted with tissue processing. MDW is a student in the Department of Neurobiology & Anatomy and Medical Scientist Training Program at the University of Rochester School of Medicine & Dentistry. Supported by NIH Research Award RO1 AG030149 and NIGMS T32 GM07356.

References

Allan SM, Tyrrell PJ, Rothwell NJ. Interleukin-1 and neuronal injury. Nat Rev Immunol. 2005; 5:629–640. [PubMed: 16034365]

Ben Menachem-Zidon O, Goshen I, Kreisel T, Ben Menahem Y, Reinhartz E, Ben Hur T, Yirmiya R. Intrahippocampal transplantation of transgenic neural precursor cells overexpressing interleukin-1 receptor antagonist blocks chronic isolation-induced impairment in memory and neurogenesis. Neuropsychopharmacology. 2008; 33:2251–2262. [PubMed: 17987063]

Burger C, Gorbatyuk OS, Velardo MJ, Peden CS, Williams P, Zolotukhin S, Reier PJ, Mandel RJ, Muzyczka N. Recombinant AAV viral vectors pseudotyped with viral capsids from serotypes 1, 2, and 5 display differential efficiency and cell tropism after delivery to different regions of the central nervous system. Mol Ther. 2004; 10:302–317. [PubMed: 15294177]

Cao L, Jiao X, Zuzga DS, Liu Y, Fong DM, Young D, During MJ. VEGF links hippocampal activity with neurogenesis, learning and memory. Nat Genet. 2004; 36:827–835. [PubMed: 15258583]

Clark PJ, Brzezinska WJ, Thomas MW, Ryzhenko NA, Toshkov SA, Rhodes JS. Intact neurogenesis is required for benefits of exercise on spatial memory but not motor performance or contextual fear conditioning in C57BL/6J mice. Neuroscience. 2008; 155:1048–1058. [PubMed: 18664375]

Cunningham ET Jr, Wada E, Carter DB, Tracey DE, Battey JF, De Souza EB. In situ histochemical localization of type I interleukin-1 receptor messenger RNA in the central nervous system, pituitary, and adrenal gland of the mouse. J Neurosci. 1992; 12:1101–1114. [PubMed: 1532025]

David DJ, Samuels BA, Rainer Q, Wang JW, Marsteller D, Mendez I, Drew M, Craig DA, Guiard BP, Guilloux JP, Artymyshyn RP, Gardier AM, Gerald C, Antonijevic IA, Leonardo ED, Hen R. Neurogenesis-dependent and -independent effects of fluoxetine in an animal model of anxiety/depression. Neuron. 2009; 62:479–493. [PubMed: 19477151]

Davidson BL, Stein CS, Heth JA, Martins I, Kotin RM, Derksen TA, Zabner J, Ghodsi A, Chiorini JA. Recombinant adeno-associated virus type 2, 4, and 5 vectors: transduction of variant cell types and regions in the mammalian central nervous system. Proc Natl Acad Sci USA. 2000; 97:3428–3432. [PubMed: 10688913]

Deng W, Saxe MD, Gallina IS, Gage FH. Adult-born hippocampal dentate granule cells undergoing maturation modulate learning and memory in the brain. J Neurosci. 2009; 29:13532–13542. [PubMed: 19864566]

Encinas JM, Vaahtokari A, Enikolopov G. Fluoxetine targets early progenitor cells in the adult brain. Proc Natl Acad Sci USA. 2006; 103:8233–8238. [PubMed: 16702546]

Frisen J, Johansson CB, Torok C, Risling M, Lendahl U. Rapid, widespread, and longlasting induction of nestin contributes to the generation of glial scar tissue after CNS injury. J Cell Biol. 1995; 131:453–464. [PubMed: 7593171]

Gemma C, Bachstetter AD, Cole MJ, Fister M, Hudson C, Bickford PC. Blockade of caspase-1 increases neurogenesis in the aged hippocampus. Eur J Neurosci. 2007; 26:2795–2803. [PubMed: 18001276]

Goshen I, Kreisel T, Ben-Menachem-Zidon O, Licht T, Weidenfeld J, Ben-Hur T, Yirmiya R. Brain interleukin-1 mediates chronic stress-induced depression in mice via adrenocortical activation and hippocampal neurogenesis suppression. Mol Psychiatry. 2008; 13:717–728. [PubMed: 17700577]

Hein AM, Stasko MR, Matousek SB, Scott-McKean JJ, Maier SF, Olschowka JA, Costa AC, O'Banion MK. Sustained hippocampal IL-1beta overexpression impairs contextual and spatial memory in transgenic mice. Brain Behav Immun. 2010; 24:243–253. [PubMed: 19825412]

Hein AM, Zarcone TJ, Parfitt DB, Matousek SB, Carbonari DM, Olschowka JA, O'Banion MK. Behavioral, structural and molecular changes following long-term hippocampal IL-1beta overexpression in transgenic mice. J Neuroimmune Pharmacol. 2012; 7:145–155. [PubMed: 21748283]

Iosif RE, Ekdahl CT, Ahlenius H, Pronk CJ, Bonde S, Kokaia Z, Jacobsen SE, Lindvall O. Tumor necrosis factor receptor 1 is a negative regulator of progenitor proliferation in adult hippocampal neurogenesis. J Neurosci. 2006; 26:9703–9712. [PubMed: 16988041]

Janelsins MC, Mastrangelo MA, Park KM, Sudol KL, Narrow WC, Oddo S, LaFerla FM, Callahan LM, Federoff HJ, Bowers WJ. Chronic neuron-specific tumor necrosis factor-alpha expression enhances the local inflammatory environment ultimately leading to neuronal death in 3xTg-AD mice. Am J Pathol. 2008; 173:1768–1782. [PubMed: 18974297]

Kaneko N, Sawamoto K. Adult neurogenesis and its alteration under pathological conditions. Neurosci Res. 2009; 63:155–164. [PubMed: 19118585]

Koo JW, Duman RS. IL-1beta is an essential mediator of the antineurogenic and anhedonic effects of stress. Proc Natl Acad Sci USA. 2008; 105:751–756. [PubMed: 18178625]

Lagace DC, Donovan MH, Decarolis NA, Farnbauch LA, Malhotra S, Berton O, Nestler EJ, Krishnan V, Eisch AJ. Adult hippocampal neurogenesis is functionally important for stress-induced social avoidance. Proc Natl Acad Sci USA. 2010; 107:4436–4441. [PubMed: 20176946]

Lagace DC, Whitman MC, Noonan MA, Ables JL, DeCarolis NA, Arguello AA, Donovan MH, Fischer SJ, Farnbauch LA, Beech RD, DiLeone RJ, Greer CA, Mandyam CD, Eisch AJ. Dynamic contribution of nestin-expressing stem cells to adult neurogenesis. J Neurosci. 2007; 27:12623–12629. [PubMed: 18003841]

Leuner B, Mendolia-Loffredo S, Kozorovitskiy Y, Samburg D, Gould E, Shors TJ. Learning enhances the survival of new neurons beyond the time when the hippocampus is required for memory. J Neurosci. 2004; 24:7477–7481. [PubMed: 15329394]

Lin RC, Matesic DF, Marvin M, McKay RD, Brustle O. Re-expression of the intermediate filament nestin in reactive astrocytes. Neurobiol Dis. 1995; 2:79–85. [PubMed: 8980011]

Madisen L, Zwingman TA, Sunkin SM, Oh SW, Zariwala HA, Gu H, Ng LL, Palmiter RD, Hawrylycz MJ, Jones AR, Lein ES, Zeng H. A robust and high-throughput Cre reporting and characterization system for the whole mouse brain. Nat Neurosci. 2010; 13:133–140. [PubMed: 20023653]

McPherson CA, Aoyama M, Harry GJ. Interleukin (IL)-1 and IL-6 regulation of neural progenitor cell proliferation with hippocampal injury: differential regulatory pathways in the subgranular zone (SGZ) of the adolescent and mature mouse brain. Brain Behav Immun. 2011; 25:850–862. [PubMed: 20833246]

Monje ML, Toda H, Palmer TD. Inflammatory blockade restores adult hippocampal neurogenesis. Science. 2003; 302:1760–1765. [PubMed: 14615545]

Moore AH, Wu M, Shaftel SS, Graham KA, O'Banion MK. Sustained expression of interleukin-1beta in mouse hippocampus impairs spatial memory. Neuroscience. 2009; 164:1484–1495. [PubMed: 19744544]

Pfaffl MW. A new mathematical model for relative quantification in real-time RT-PCR. Nucleic Acids Res. 2001; 29:e45. [PubMed: 11328886]

Rolls A, Shechter R, London A, Ziv Y, Ronen A, Levy R, Schwartz M. Toll-like receptors modulate adult hippocampal neurogenesis. Nat Cell Biol. 2007; 9:1081–1088. [PubMed: 17704767]

Ryan DA, Mastrangelo MA, Narrow WC, Sullivan MA, Federoff HJ, Bowers WJ. Abeta-directed single-chain antibody delivery via a serotype-1 AAV vector improves learning behavior and pathology in Alzheimer's disease mice. Mol Ther. 2010; 18:1471–1481. [PubMed: 20551911]

Sahay A, Hen R. Adult hippocampal neurogenesis in depression. Nat Neurosci. 2007; 10:1110–1115. [PubMed: 17726477]

Seri B, Garcia-Verdugo JM, McEwen BS, Alvarez-Buylla A. Astrocytes give rise to new neurons in the adult mammalian hippocampus. J Neurosci. 2001; 21:7153–7160. [PubMed: 11549726]

Shaftel SS, Carlson TJ, Olschowka JA, Kyrkanides S, Matousek SB, O'Banion MK. Chronic interleukin-1beta expression in mouse brain leads to leukocyte infiltration and neutrophil-independent blood brain barrier permeability without overt neurodegeneration. J Neurosci. 2007a; 27:9301–9309. [PubMed: 17728444]

Shaftel SS, Kyrkanides S, Olschowka JA, Miller JN, Johnson RE, O'Banion MK. Sustained hippocampal IL-1 beta overexpression mediates chronic neuroinflammation and ameliorates Alzheimer plaque pathology. J Clin Invest. 2007b; 117:1595–1604. [PubMed: 17549256]

Shors TJ, Miesegaes G, Beylin A, Zhao M, Rydel T, Gould E. Neurogenesis in the adult is involved in the formation of trace memories. Nature. 2001; 410:372–376. [PubMed: 11268214]

Sims JE, Smith DE. The IL-1 family: regulators of immunity. Nat Rev Immunol. 2010; 10:89–102. [PubMed: 20081871]

Takeda K, Akira S. TLR signaling pathways. Semin Immunol. 2004; 16:3–9. [PubMed: 14751757]

Urabe M, Ding C, Kotin RM. Insect cells as a factory to produce adeno-associated virus type 2 vectors. Hum Gene Ther. 2002; 13:1935–1943. [PubMed: 12427305]

Vallieres L, Campbell IL, Gage FH, Sawchenko PE. Reduced hippocampal neurogenesis in adult transgenic mice with chronic astrocytic production of interleukin-6. J Neurosci. 2002; 22:486–492. [PubMed: 11784794]

van Praag H, Christie BR, Sejnowski TJ, Gage FH. Running enhances neurogenesis, learning, and long-term potentiation in mice. Proc Natl Acad Sci USA. 1999; 96:13427–13431. [PubMed: 10557337]

Wesche H, Henzel WJ, Shillinglaw W, Li S, Cao Z. MyD88: an adapter that recruits IRAK to the IL-1 receptor complex. Immunity. 1997; 7:837–847. [PubMed: 9430229]

Wingren AG, Bjorkdahl O, Labuda T, Bjork L, Andersson U, Gullberg U, Hedlund G, Sjogren HO, Kalland T, Widegren B, Dohlsten M. Fusion of a signal sequence to the interleukin-1 beta gene directs the protein from cytoplasmic accumulation to extracellular release. Cell Immunol. 1996; 169:226–237. [PubMed: 8620550]

Wu MD, Hein AM, Moravan MJ, Shaftel SS, Olschowka JA, O'Banion MK. Adult murine hippocampal neurogenesis is inhibited by sustained IL-1beta and not rescued by voluntary running. Brain Behav Immun. 2012; 26:292–300. [PubMed: 21983279]

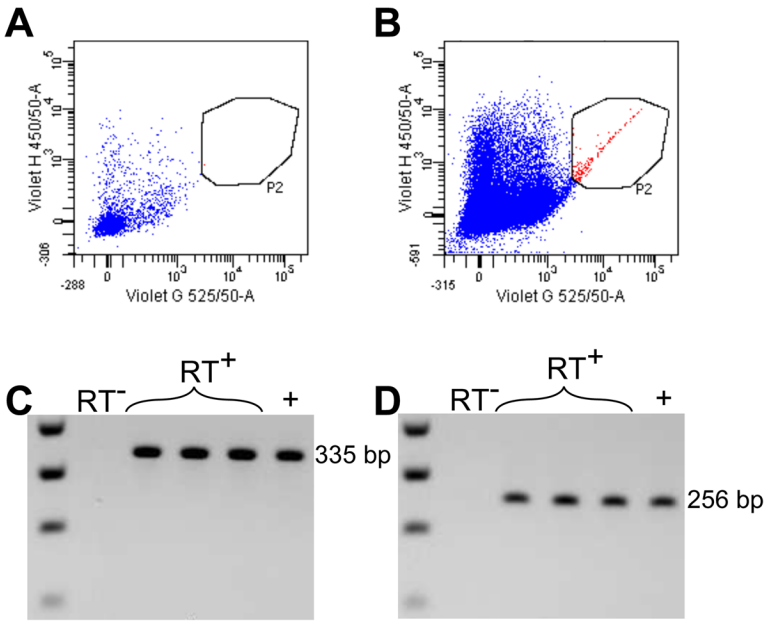

Fig. 1.

MyD88 and IL-1R1 are expressed by CFP$^+$ cells isolated from nestin-CFPnuc mice. Gating on CFP$^+$ cells from WT or nestin-CFPnuc mice (A, B respectively, cells pooled from 2 animals/group). Detection of MyD88 (C) and IL-1R1 (D) cDNA after reverse transcription of sorted CFP$^+$ cells. RT$^-$ = no reverse transcriptase, RT$^+$ = reverse transcriptase, + = positive control.

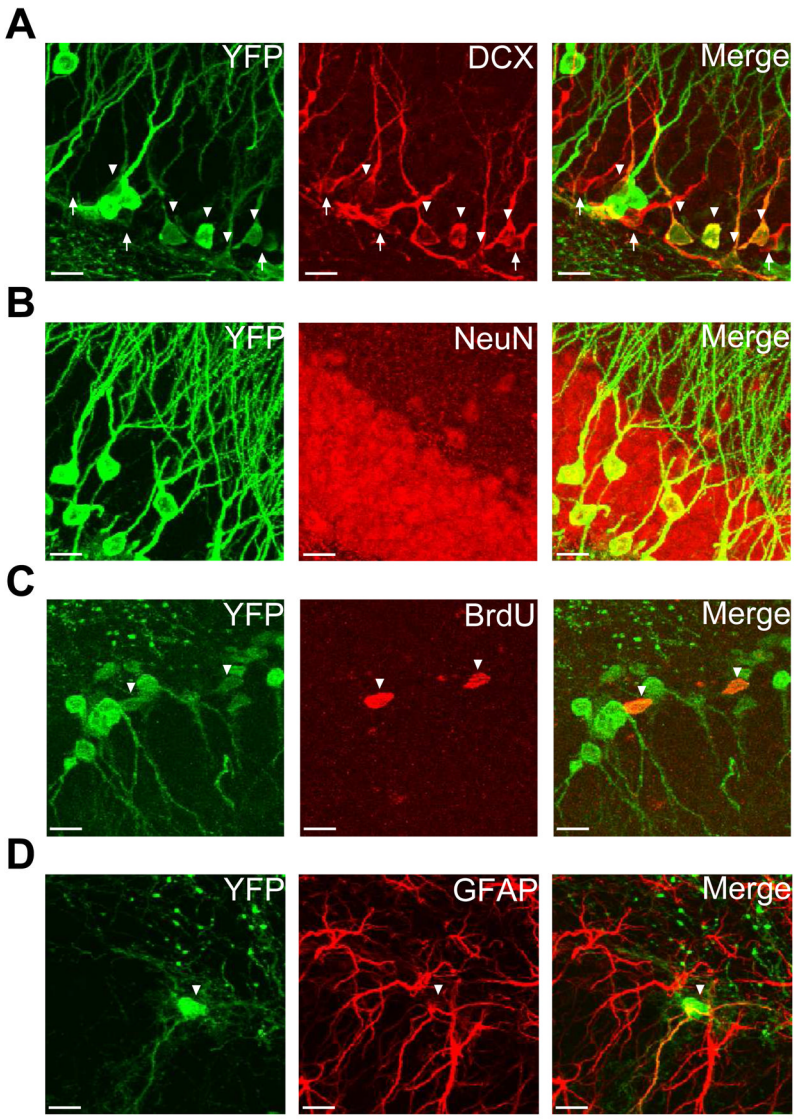

Fig. 2.

Nestin-CreER^{T2}, Ai3-YFP: inducible and conditional genetic fate mapping model. Representative staining of YFP (green) from nestin-CreERT2, Ai3-YFP mice and DCX (red) showing DCX^{+}YFP^{+} cells (A). Mature neurons can be identified by expression of NeuN (B). Neural precursors are identified by incorporation of BrdU that was given 2 hours before sacrifice (C) and expression of GFAP (D). Double-positive cells are indicated by arrow heads. DCX^{+}YFP^{-} cells are indicated by white arrows. Scale bars = 10 μm.

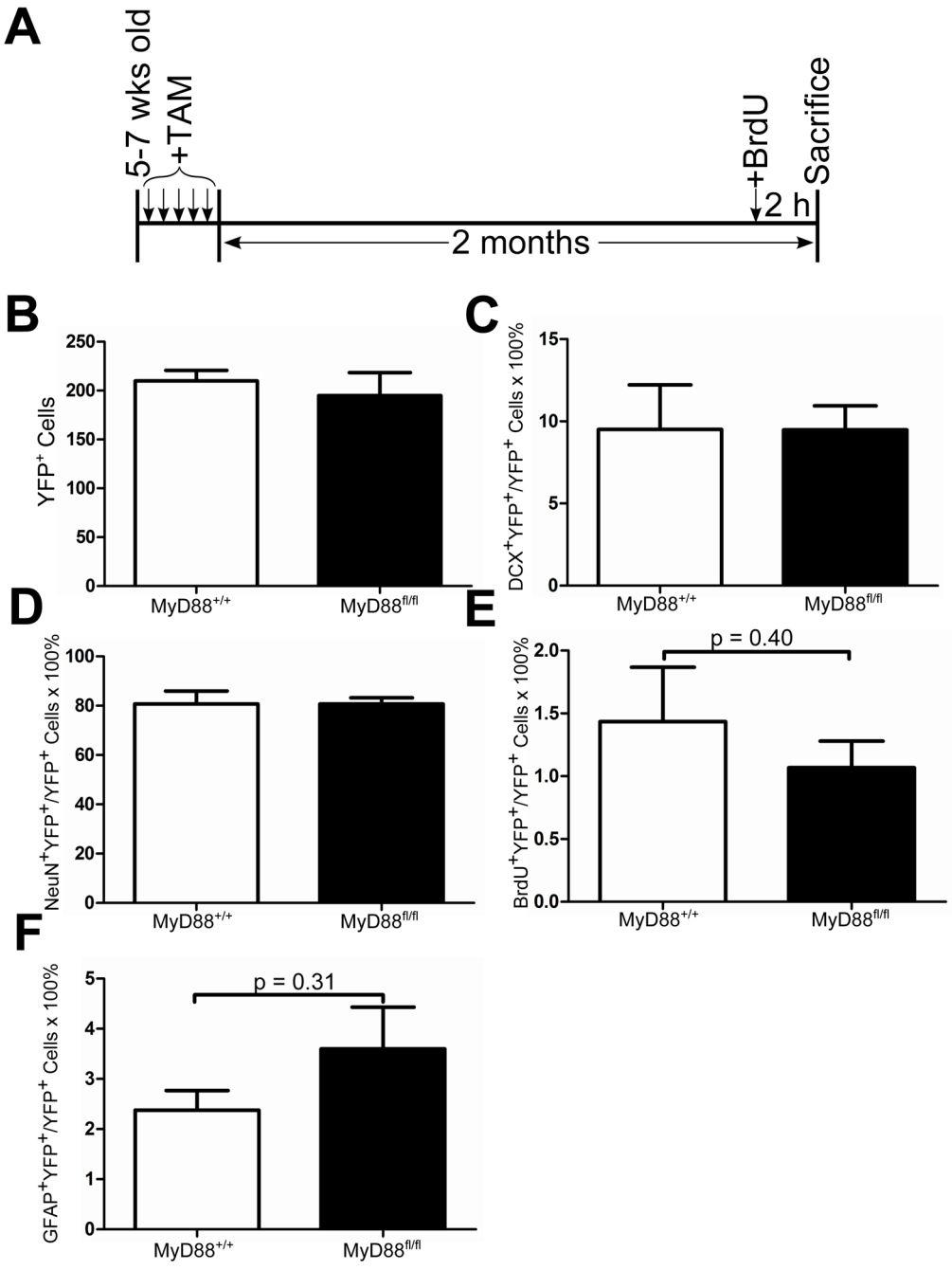

Fig. 3.

Normal adult neurogenesis is unaltered by conditional knockout of MyD88 in nestin^{+} cells. Experimental design depicting timeline for dosing of 180 mg/kg tamoxifen (TAM) and 50 mg/kg BrdU intraperitoneal injections for nestin-CreER^{T2},YFP (MyD88$^{+/+}$) and nestin-CreER^{T2},YFP,MyD88$^{fl/fl}$ (MyD88$^{fl/fl}$) mice (A). Quantification of total number of YFP^{+} cells (B), DCX^{+}YFP^{+} neuroblasts (C), NeuN^{+}YFP^{+} neurons (D), BrdU^{+}YFP^{+} proliferating cells (E), and GFAP^{+}YFP^{+} neural precursors (F) at 2 months after tamoxifen cessation. n = 6–12 animals/group. Two-tailed Student's t-test. Data represent means ± SEM.

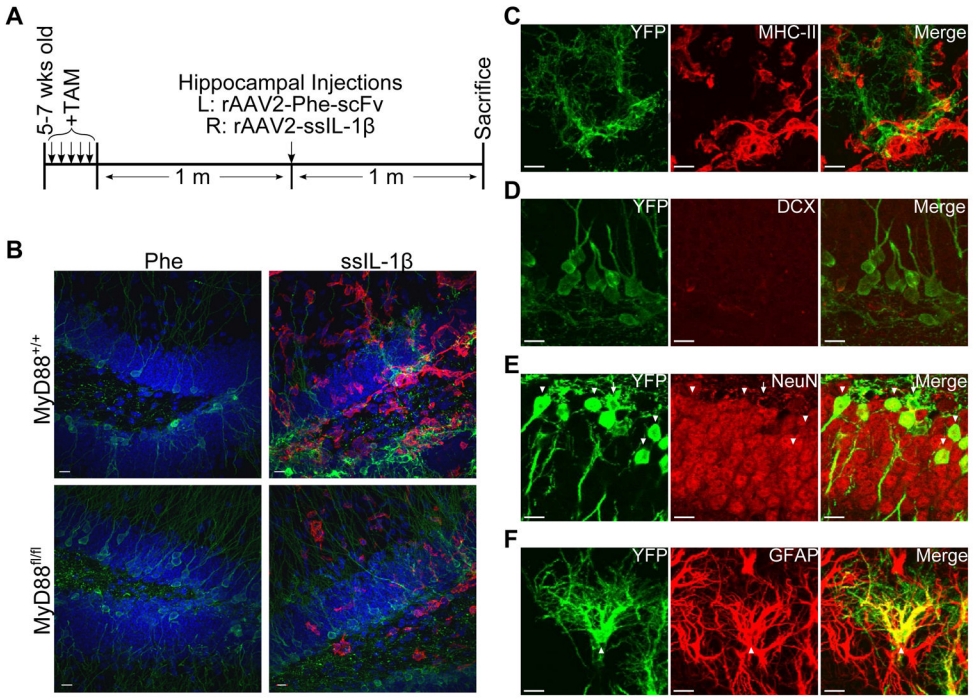

Fig. 4.

Alteration of cell fate by rAAV2-ssIL-1β induced inflammation. Experimental design showing tamoxifen (TAM) administration as well as intrahippocampal injections (A). MHC-II (red) staining demonstrating unilateral nature of inflammation in addition to YFP^+ (green) cells in hippocampi that received ssIL-1β (B,C). Co-labeling of YFP^+ cells with DCX to label neuroblasts (D), NeuN to label neurons (E), and GFAP to label reactive astrocytes (F). Arrowheads indicate double positive cells. Arrow indicates a $NeuN^-YFP^+$ cell. Scale bars = 10 μm.

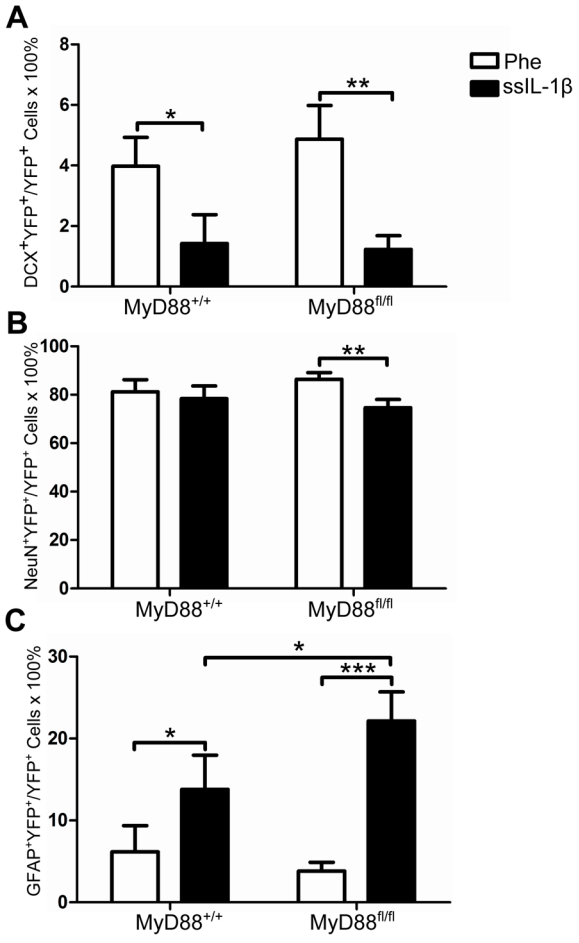

Fig. 5.

Loss of MyD88 in nestin$^+$ cells and their progeny does not rescue the reduction in neurogenesis due to rAAV2-ssIL-1β. Quantification of the proportion of YFP$^+$ that are DCX$^+$ neuroblasts (**G**), NeuN$^+$ neurons (**H**), and GFAP$^+$ reactive astrocytes (**I**). n = 6–12 animals/group, * = $p < 0.05$, ** = $p < 0.01$, *** = $p < 0.001$, 2-way ANOVA using a post-hoc test with a one-tailed Bonferroni adjustment. Data represent means ± SEM.

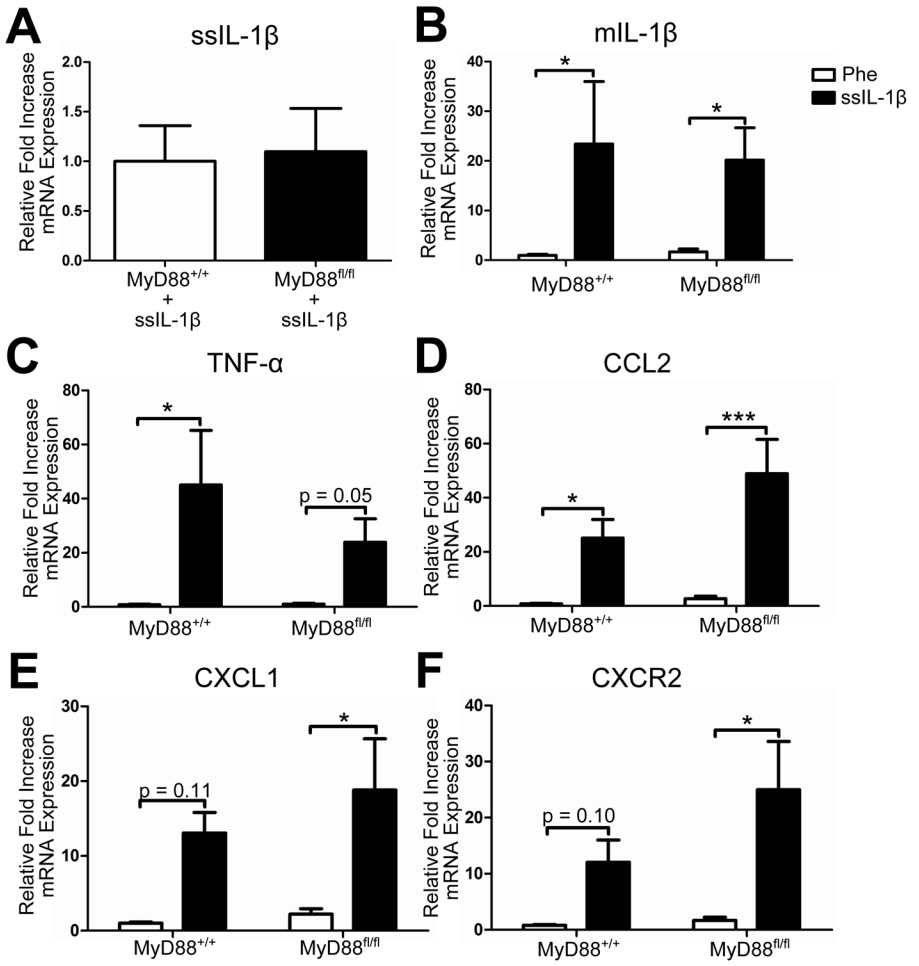

Fig. 6.

Inflammatory transcript levels are similar in rAAV2-ssIL-1β transduced MyD88$^{fl/fl}$ versus MyD88$^{+/+}$ mice. MyD88$^{+/+}$ and MyD88$^{fl/fl}$ mice received intrahippocampal injections of rAAV2-Phe-scFv and –ssIL-1β one month after cessation of tamoxifen and were sacrificed one month later. RNA was isolated from microdissected hippocampi and reverse transcribed. Quantitative real-time PCR for ssIL-1β from –ssIL-1β injected hippocampi (A). ssIL-1β could not be detected in hippocampi that received –Phe. Increases in mRNA expression relative to MyD88$^{+/+}$-Phe shown for murine IL-1β (B), TNF-α (C), CCL2 (D), CXCL1 (E), and CXCR2 (F). All samples were standardized to 18S as a housekeeping gene. n = 6–7 animals/group. Unpaired two-tailed Student's t-test was used for ssIL-1β transcript levels. 2-way ANOVA with matching and post-hoc test with a one-tailed Bonferroni adjustment was used for all other genes. * = $p < 0.05$, *** = $p < 0.001$. Data represent means ± SEM.

Table 1

Primary antibodies for immunohistochemistry.

Antigen	Company	Catalog Number	Dilution(s)
MHC-II	BD Pharmingen	556999	1:2000
DCX	Santa Cruz	sc-8066	1:1000
BrdU	Abcam	ab6326	1:300
NeuN	Chemicon	MAB377B	1:2000
GFAP	Dako	Z0334	1:2000
GFAP	Sigma-Aldrich	C-9205	1:1000
GFP	Invitrogen	A-6455	1:4000
GFP	Invitrogen	A-21311	1:200
Iba-1	Wako	016-20001	1:2000
Ly6B.2	Serotec	MCA771G	1:2000
MyD88	Abcam	ab2064	1:500

Table 2

Primer sequences for q-RT-PCR.

Gene 5′ → 3′	Forward	Reverse	Probe
18S	cgaccataaacgatgccgac	gtggtgcccttccgtcaa	cggcggcgttattcccatgacc
CXCR2	gtctttcagcatggctcattac	cgtgacctctttctccctgta	agactgtggtatttgaattgatgcagcc
mIL-1β	tcgctcagggtcacaagaaa	atcagaggcaaggaggaaacac	catggcacattctgttcaaagagagcctg
ssIL-1β	gcctccgcagtcacctaat	ggtggagagctttcagttcata	agacgatctgcgcacctgtacgat
CXCL1	gctaaaaggtgtccccaagtaa	taggaccctcaaaagaaattgta	ctgctctgatggcaccgtctggt
CCL2	ggctcagccagatgcagttaa	cctactcattgggatcatcttgct	ccccactcacctgctgctactcattca
TNF-α	gacaaggctgccccgacta	tttctcctggtatgagatagcaaatc	ctcctcacccacaccgtcagcc